Title
NEUTRON EMISSION FOLLOWING u-MESON CAPTURE IN SILVER AND LEAD

Authors
Kaplan, Selig N.
Mover, Burton J.
Pyle, Robert V.

Publication Date
1957-11-11

UNIVERSITY OF CALIFORNIA

Radiation Laboratory

BERKELEY, CALIFORNIA

DISCLAIMER

UCRL-3749 Rev.

UNIVERSITY OF CALIFORNIA
Radiation Laboratory
Berkeley, California

Contract No. W-7405-eng-48

NEUTRON EMISSION FOLLOWING μ-MESON CAPTURE IN SILVER AND LEAD

Selig N. Kaplan, Burton J. Moyer, and Robert V. Pyle

November 11, 1957

Printed for the U. S. Atomic Energy Commission

NEUTRON EMISSION FOLLOWING μ-MESON CAPTURE IN SILVER AND LEAD

Selig N. Kaplan, Burton J. Moyer, and Robert V. Pyle

Radiation Laboratory
University of California
Berkeley, California

November 11, 1957

ABSTRACT

The neutron yield from the capture of cosmic-ray μ^- mesons in silver and lead has been measured by use of a high-efficiency Cd-loaded liquid-scintillator tank. The average multiplicities were determined to be $\bar{\nu}_{Ag} = 1.60 \pm 0.18$ and $\bar{\nu}_{Pb} = 1.64 \pm 0.16$.

The multiplicity distributions were also measured and compared with several theoretical models. Although an α-particle model gave results not inconsistent with the data, a Fermi gas model with the effective nucleon mass M^* set equal to $M/2$ seemed to provide the better fit.

NEUTRON EMISSION FOLLOWING μ-MESON CAPTURE IN SILVER AND LEAD

Selig N. Kaplan, Burton J. Moyer, and Robert V. Pyle

Radiation Laboratory
University of California
Berkeley, California

November 11, 1957

I. INTRODUCTION

Recent theoretical nuclear models predict that inside a nucleus a nucleon exhibits an "effective mass" that is only half as large as its free rest mass, M.[1-3] An attempt has been made to observe this effect by use of the μ^- meson as a nuclear probe.

For example, if a μ meson were to interact at rest with a proton, $\mu^- + p \rightarrow n + \nu$, a solution of this simple kinematic problem shows that the neutron would recoil with some 5 Mev of kinetic energy. If this interaction occurred inside a complex nucleus, however, and if nucleons exhibited the reduced "effective mass," M/2, then the neutron would recoil with a kinetic energy of 10 Mev in the rest frame of the interaction.

The μ meson stopping in condensed material is trapped in a Bohr orbit about a nucleus. In a time that is very short compared with its decay lifetime, it falls into the K orbit[4] (the mesic x-rays predicted to be associated with this effect[5,6] are indeed observed[7]), and from there either decays or interacts with the nucleus.

The now classic experiment of Conversi, Pancini, and Piccioni[8] gave the first evidence of this competition between decay and capture. In later experiments, the μ lifetimes were measured over a large spectrum of atomic numbers,[9] and they were found to be quite compatible with an interaction of the form of electron K capture, i.e., $\mu^- + Z^A \rightarrow (Z-1)^A + \nu$.[5-10] The nature of the interaction is also verified by experiments designed to observe the reaction products. No photons with energy more than 20 Mev and no electrons are observed;[11-13] a very few protons have been observed ($\simeq 0.025$ per capture in Ag and Br);[14] and it is indicated that one to two neutrons are emitted per interaction.[15-20] These results confirm the interaction assumed

above; that is, most of the rest energy of the μ meson is carried off in an undetectable way (the neutrino), and the residual nucleus is excited to some 10 to 20 Mev, enough to "boil off" one or two neutrons but not enough to enable many protons to penetrate the Coulomb barrier.

Unfortunately, it is very difficult to measure the excitations directly, but we can measure the neutron-multiplicity distribution and then interpret this in terms of a nuclear-excitation distribution.

The neutron-detection experiments, which are of particular interest to us, may be subdivided into three categories. The earliest experiments, in 1948, indicated a correlation between stopping μ mesons and neutrons.[15,16] Later work, up to 1951, by the same experimenters and collaborators[17] showed the neutron multiplicities to be at least qualitatively in agreement with the neutrino assumption and the excitation distributions calculated by Tiomno and Wheeler[21] and by Rosenbluth.[22]

The third group of experiments however, characterized by better statistics and greater neutron-counting efficiencies,[18-20] seemed to indicate neutron multiplicities greater than were expected on the basis of the theoretical calculations.

If a two-body interaction is assumed, $\mu^- + p \rightarrow n + \nu$, the nuclear-excitation distribution is determined by the proton momentum and energy distribution in the nucleus. The early theoretical work on the problem assumed a nucleon-momentum distribution characteristic of a completely degenerate Fermi gas.[21,22] Two modifications have been proposed to explain these higher multiplicities. One of these by Lang,[23] leaves the momentum distribution unchanged but suggests that $p^2/2M$ be set equal to E/γ ($E \equiv$ nucleon kinetic energy), rather than E, where γ is a constant with a value between 1.5 and 2, p is the nucleon momentum, and M is mass. This has the effect of associating a higher energy with a given momentum in the sense that the effective nucleon mass is reduced by the factor $1/\gamma$.

The other proposal, by Cole,[24] suggests modification of the nucleon-momentum distribution to one with a high momentum tail. This distribution is obtained by assuming the initial proton to be part of an α-particle subunit inside the nucleus.

These models can be adjusted to predict the same average number of neutrons but not the same multiplicity distribution. They are discussed in greater detail later in this paper, and their predicted distributions are

compared with our experimental results.

Because of low neutron-detection efficiency the previous experiments could not yield much useful information on multiplicity distribution. The most efficient scheme (which was better by a factor of two than any of the others) gave a detection efficiency of only 7%.[20] On the other hand, we had available a large cadmium-loaded liquid-scintillator tank that could be employed in a 4π geometry about a target. In a slightly different application, the tank had exhibited fission-neutron-detection efficiencies as high as 77%,[25] and the large volume of the tank makes its efficiency almost insensitive to neutron energy over a large range of values.[25]

An excellent review of the experimental and theoretical work on the nuclear interaction of μ mesons through 1952, together with additional references, can be found in an article by Sard and Crouch.[24]

II. THEORY

After a μ^- meson has been absorbed by a nucleus and a neutrino has been emitted, $(\mu^- + Z^A \rightarrow (Z-1)^{A*} + \nu)$, the excited product nucleus decays primarily by emission of neutrons. A measurement of the number of neutrons emitted following μ^- capture provides a lower limit to the amount of energy imparted to nuclear matter. This limit is the mass difference between the $(Z-1)^A$ nucleus and the Z^A target nucleus plus the binding energies of the observed number of neutrons to the $(Z-1)^A$ product nucleus. The amount of excitation is, in turn, related to the mechanism of the capture and the mutual interactions of the nucleons. Thus, to make quantitative predictions about the neutron yield from μ^- meson capture, we must first determine the induced nuclear excitation and then relate this excitation to neutron multiplicities.

A. Nuclear Excitation

1. Fermi Gas Model

We may write general conservation equations for the interaction of a stopped μ meson with the nucleus, Z^A:

$$\mu' c^2 = p_\nu c + \Delta M c^2 + Q \qquad (1)$$

and

$$\vec{p}_\nu + \vec{p}_{Z-1}^{\,A} = 0 \qquad (2)$$

where $\vec{p}_\nu$ and $\vec{p}^{\,A}_{Z-1}$ are the momenta of the neutrino and the resultant nucleus respectively; $\mu' c^2$ is the rest energy of the μ meson reduced by its K-shell binding energy; Q represents both the excitation and kinetic energy of the $(Z-1)^A$ nucleus; and $\Delta M c^2$ is the difference in rest energy between the $(Z-1)^A$ and Z^A nuclei. It is convenient to define E_0 as the total energy available for excitation of the product nucleus and rewrite Eq. (1) as

$$\mu' c^2 - \Delta M c^2 \equiv E_0 = p_\nu c + Q. \qquad (1)'$$

Two assumptions are made in applying this model to find the nuclear excitation; first, that the μ meson interacts with a single proton of momentum $\vec{p}$, transforming it into a neutron of momentum $\vec{q}$; and second, that the nucleus behaves like a Fermi gas, its ground state being completely degenerate. The first of these assumptions allows us to write

$$\vec{p}_\nu + \vec{q} + \vec{p}^{\,A-1}_{Z-1} = 0,$$

where $\vec{p}^{\,A-1}_{Z-1}$ is the momentum of the "core" nucleus, composed of the A - 1 nucleons assumed not to participate in the interaction. The "core" therefore maintains its initial momentum, which is equal in magnitude but opposite in direction to that of the capturing proton. Hence, the momentum-conservation equation, (2), becomes

$$\vec{p}_\nu + \vec{q} - \vec{p} = 0. \qquad (2)'$$

The kinetic energy of the resultant nucleus is smaller than its excitation by a factor $O(1/A)$; therefore we shall neglect it and consider Q to be the nuclear excitation.

The interaction probability is proportional to the density of final states, $\left.\frac{dn}{dE}\right|_{E_0}$:

$$\left.\frac{dn}{dE}\right|_{E_0} \propto \int d^3\vec{p}_\nu \, d^3\vec{q} \, d^3\vec{p} \, \delta(\vec{p}_\nu + \vec{q} - \vec{p}) \, \delta(E_0 - p_\nu c - Q),$$

where the δ functions provide for conservation of energy and momentum. It is understood that $d^3\vec{p}$ is integrated only over the occupied proton states and,

because of the exclusion principle, $d^3\vec{q}$ only over the unoccupied neutron states. In practice, these latter constraints are placed on the integration by means of distribution-density functions, $f(\vec{p})$ and $g(\vec{q})$, which are equal to the probability per unit volume of momentum space for finding a proton and a neutron respectively. Thus we have

$$\left.\frac{dn}{dE}\right|_{E_0} \propto \int d^3\vec{p}_\nu \, d^3\vec{q} \, d^3\vec{p} \, f(\vec{p}) \, [\,1 - g(\vec{q})\,] \, \delta(\vec{p}_\nu + \vec{q} - \vec{p}) \, \delta(E_0 - p_\nu c - Q), \quad (3)$$

where the integral is now taken over all momentum space.

We relate Q to the momenta by assuming that in a Fermi gas nucleus the ground state of $(Z-1)^A$ is achieved by the transformation of a proton on the surface of the Fermi momentum sphere ($p = p_o$) into a neutron on the surface ($q = q_o$). Therefore the nuclear excitation Q may be expressed as

$$\begin{aligned} Q &= (q^2 - p^2)/2M^* - (q_o^2 - p_o^2)/2M^* \\ &\equiv \Delta T' - \Delta T, \end{aligned} \quad (4)$$

M^* being the effective nucleon mass. Substitution of Eqs. (2)' and (4) into (1)' gives

$$E_0 = p_\nu c - \Delta T + (p_\nu^2 - 2\vec{p} \cdot \vec{p}_\nu)/2M^* \quad (1)''$$

For a strongly degenerate Fermi gas, f and g have the forms

$$f = \left\{ \exp (p^2 - p_o^2)/2M^*\theta_F + 1 \right\}^{-1},$$

$$g = \left\{ \exp (q^2 - q_o^2)/2M^*\theta_F + 1 \right\}^{-1},$$

where θ_F is the Fermi temperature (in Mev). Substitution of these into Eq. (3) and integration over all variables but p_ν gives

$$\left.\frac{dn}{dE}\right|_{E_0} \propto \int p_\nu \, dp_\nu \, [\,1 - \exp(-E_0 + p_\nu c)/2\theta_F\,]^{-1} \times \ell n \left\{ [\,1 + \exp(a + E_0 - p_\nu c)/2\theta_F\,] \Big/ [\,1 + \exp(a - E_0 + p_\nu c)/2\theta_F\,] \right\},$$

where

$$a \equiv (q_o^2 + p_o^2)/2M^* - p_\nu^2/4M^* - M^*(E_0 - p_\nu c + \Delta T)^2/p_\nu^2.$$

Making a change of variable to Q (since $p_\nu c = E_0 - Q$), we have

$$\left.\frac{dn}{dE}\right|_{E_0} \propto \int (E_0 - Q)\,[1 - \exp(-Q/\theta_F)]^{-1} \times \ln\left\{[1 + \exp(a + Q)/2\theta_F]/[1 + \exp(a - Q)/2\theta_F]\right\} dQ.$$

This is of the form

$$\left.\frac{dn}{dE}\right|_{E_0} \propto \int I(Q)\, dQ,$$

where I(Q) is the probability per unit energy of the interaction's giving a nuclear excitation Q. Therefore we may identify

$$I(Q) = 2\theta_F K (E_0 - Q)\,[1 - \exp(-Q/\theta_F)]^{-1} \times \ln\left\{[1 + \exp(a + Q)/2\theta_F]/[1 + \exp(a - Q)/2\theta_F]\right\}, \tag{5}$$

where K is the normalization constant defined by

$$\int I(Q)\, dQ = 1 .$$

In the limit, $\theta_F \to 0$

$$I(Q) = 2K(E_0 - Q)Q \qquad a - Q \geq 0, \tag{6}$$

$$= K(E_0 - Q)(a + Q) \qquad a - Q \leq 0.$$

This excitation distribution is plotted in Fig. 1 for the cases $M^* = M$ and $M^* = M/2$.

In view of experimental evidence, from lighter nuclei, for a high-momentum tail in the nucleon-momentum distribution,[26,27] and the presumption that it also exists in heavier nuclei, the excitation distribution of Eq. (4) has also been plotted for $M^* = M$, $\theta_F = 5$ Mev,[28] and $M^* = M/2$, $\theta_F = 10$ Mev (because it seemed appropriate to associate a higher temperature with the higher kinetic energies produced by a decrease in the effective nucleon mass).

2. Alpha-Particle Model

In the model employed by Cole[24] the reaction goes according to the equation

$$\mu^- + He^4 \rightarrow H^3 + n + \nu .$$

As regards momentum conservation, however, only the part $\mu^- + p \rightarrow n + \nu$ is considered. The proton is considered to be part of the He^4 initially, for the purpose of obtaining a momentum distribution with a high momentum component, and the H^3 in the final state permits application of the exclusion principle.

The energy distribution ($I(Q)$) is found from perturbation theory with the matrix element obtained from derived wave functions.

This model is designed to consider in detail the effect on the interaction of neighboring nucleons although neglecting the rest of the nucleus. Emphasizing the effect of close interactions allows for higher proton momentum, thus making possible higher-energy transfers. The predicted excitation-distribution curve taken from Cole[24] is also shown in Fig. 1.

B. Neutron Emission

In order to interpret the excitation in terms of observed neutron multiplicities, we assume that this excitation, initially in the form of neutron kinetic energy, is quickly shared with other nucleons to produce a "thermally" excited nucleus (the "Bohr assumption").

It is assumed that neutrons are then "boiled off" from the excited nucleus with an energy spectrum of the form[27, 28]

$$N(\epsilon) \propto \epsilon \exp(-\epsilon/\Theta),$$

where $\epsilon \equiv$ neutron kinetic energy,

$\Theta \equiv$ a constant that depends upon the nuclear excitation.
(For our purposes, we felt it was sufficient to approximate this constant as 0.75 Mev.)[29, 30]

The nucleus will continue to emit neutrons until there is not enough excitation left to emit more, and only then will it decay to its ground state by emission of γ radiation. We have assumed that the proton emission is negligible.[14, 29]

If the nuclear excitation is in excess of the binding energy of ν neutrons,

B_ν, by an amount $\delta_\nu\Theta = Q - B_\nu$, ν or more neutrons will be emitted, providing the total kinetic energy of the first $(\nu - 1)$ neutrons does not exceed $\delta_\nu\Theta$, that is,

$$\epsilon_1 + \epsilon_2 + \cdots \epsilon_{\nu-1} \leq \delta_\nu\Theta .$$

The probability of at least ν neutrons' being emitted from a nucleus excited to the energy Q can be expressed by the analytical relationship

$$N_\nu \propto \int_0^{\delta_\nu\Theta} \epsilon_{\nu-1} \exp(-\epsilon_{\nu-1}/\Theta)\, d\epsilon_{\nu-1} \int_0^{\delta_\nu\Theta-\epsilon_{\nu-1}} \epsilon_{\nu-2} \exp(-\epsilon_{\nu-2}/\Theta)\, d\epsilon_{\nu-2} \int \cdots$$

$$\cdots \int_0^{\delta_\nu\Theta-\epsilon_{\nu-1}-\cdots-\epsilon_2} \epsilon_1 \exp(-\epsilon_1/\Theta)\, d\epsilon_1)$$

Integrating this expression and normalizing so that $\lim_{\delta_\nu \to \infty} N_\nu = 1$, we obtain

$$N_\nu = 1 - \exp(-\delta_\nu) \sum_{n=0}^{2\nu-3} \delta_\nu^n/n! , \qquad (7)$$

where

$$\delta_\nu = (Q - B_\nu)/\Theta$$

and $B_\nu \equiv$ binding energy of ν neutrons in the original nucleus.

The probability, therefore, of emission of ν neutrons is $N_\nu - N_{\nu+1}$. Figure 2 shows N_ν plotted vs δ_ν for $\nu = 1$, 2, 3, and 4.

For multiplicities greater than three, as are predicted by Cole's model, we employed his approximation that the number of neutrons emitted from a nucleus excited to an energy Q is proportional to Q,

$$\nu(Q) \propto Q ,$$

where the proportionality constant was assumed[31] to be

$$1/[(B_1 + B_2)/2 + 2]$$

or

$$\nu(Q) = \left\{ 1/[(B_1 + B_2)/2 + 2] \right\} Q .$$

We then converted this to a step function with the steps of width

$$[(B_1 + B_2)/2 + 2]$$

III. EQUIPMENT AND OPERATION

A. Telescope

The experimental equipment may be considered in two parts--a cosmic ray telescope, and a neutron detector consisting of a large cadmium-loaded liquid scintillator tank. The telescope consisted of four plastic scintillation counters arranged as shown to scale in Fig. 3. A coincidence from Counters I and III triggered the sweeps of two oscilloscopes. On one of the oscilloscopes, pulses from Counters II and IV were displayed with appropriate electronic delays in order to show their rise and to separate them on the sweep. The signature of a stopping meson consisted of a triggered sweep on the oscilloscope displaying a prompt pulse of the appropriate height from Counter II,[32] but no pulse from Counter IV.

B. Scintillator Tank

1. General Physical Description

The neutron detector consisted of a tank 30 in. long and 30 in. in diameter with 1/4-in. steel walls.[25, 33] The inside surface was sprayed with a protective coat of molten aluminum and then with a mixture of aluminum oxide abrasive powder, water glass, and water to provide a highly reflective surface. It was filled with a solution of toluene mixed with cadmium propionate dissolved in methanol, p-terphenyl as a scintillator, and a spectrum shifter, POPOP.[34]

The curved surface of the tank has eighty-eight 1/4-inch-thick glass windows each 2-1/8 in. in diameter sealed with neoprene O rings. Against each window was mounted a Dumont 6292 photomultiplier tube enclosed in a soft-steel collar. The space between the tube face and the glass was filled with mineral oil in order to make good optical contact. The photomultiplier tubes were wired in parallel in two banks of 44 tubes each, with each bank observing all portions of the scintillator.

A copper electrical shield was placed around the entire phototube assembly, increasing the total diameter to 48 in. Access for the telescope counter and target assembly was provided by an 8-in.-diameter "beam tube" that went completely through the center of the tank (Fig. 3).

2. Method of Neutron Detection

Neutrons entering the scintillator are readily thermalized and then captured with a time constant characteristic of the Cd/H ratio. This ratio was set equal to 0.002 to give a time constant of about 10 μsec. The neutron is captured by Cd^{113} 95% of the time, giving a cascade γ decay with a total energy of 9.2 Mev,[35] and about 5% of the time it is captured by H^1, yielding a 2.2-Mev photon. Some fraction of this radiation converts in the tank and gives a pulse indicating the neutron capture.

The sweep circuit of the second oscilloscope was modified so that it swept exponentially, that is, the beam position x was proportional to the voltage on a charging condenser. Thus we had $x = x_0 [1 - \exp(-t/RC)]$, where RC was set approximately equal to 10 μsec, the neutron-capture lifetime. The sweep was displayed for 30 μsec, or three mean lives. Because of this technique, the neutron pulses were displayed with equal probabilities per unit length of sweep, thereby maximizing the average resolution and making corrections for "pile up" negligible.

3. Additional Role of the Tank as Part of the Telescope

Associated with a stopping meson there may or may not have been a prompt tank pulse. (For a stopping μ^- meson, a prompt tank pulse could be caused by the capture x-rays and the radiation emitted by a still-excited nucleus after it was unable to emit further neutrons.[13]) No event was accepted if the prompt tank pulse was higher than the highest neutron pulse, the inference being that the particle was either accompanied by another, or that it scattered into the tank. This is a reasonable inference because all prompt pulses from the fission calibration (Section III-C) easily satisfied this pulse-height criterion, and each of them represented the γ radiation from two excited nuclei boiling off neutrons. Furthermore, during the fission-calibration runs there is little absorbing material present to inhibit this transmission, in contrast to the large amount present for the attenuation of γ radiation produced by μ-meson capture in the lead or silver targets.

Drawings of typical oscilloscope trace pairs produced by a cosmic ray passing through the telescope are shown in Fig. 4. The pairs of traces were recorded on film; a Dumont oscilloscope camera viewed both 'scopes by means of a split-mirror arrangement. A complete electronics schematic is shown in Fig. 5.

C. Efficiency Calibration

The neutron-detection efficiency of the apparatus was determined with the aid of a sample of the spontaneously fissioning nuclide Cf^{252} in a fission chamber.[25] The telescope counters were disconnected from the circuit, and the oscilloscopes were triggered by the fission-chamber pulse. The fission pulse was displayed on one oscilloscope (Tektronix 545), and the scintillator-tank pulse on the other (Tektronix 517). The primary calibrations were made with Counter III and the target removed, and the fission chamber resting on Counter IV. This was done at times of target changing. Every two or three days during the course of the experiment a secondary calibration run was made with Counter III removed and the fission chamber resting on the target (because this was a much simpler mechanical procedure).

The desirability of frequent efficiency calibration was twofold. First, because neutron pulses were counted on the basis of an arbitrarily chosen minimum acceptable pulse height, a change in sensitivity of the system would change the efficiency. Secondly, it has been observed that after several months the cadmium salt begins to come out of solution.[25] This has the effect of decreasing the Cd/H ratio, thereby increasing the neutron-capture lifetime. Because the tank pulses are observed over a constant 30-μsec interval, the detection efficiency is decreased. Actually, the detection efficiency decreased from 59% to 51% during the course of the experiment.

D. Equipment Maintenance

The data collection took place over a 200-day period beginning April 20, 1956. The associated equipment was in constant operation except when shut down for repair.

The following stability checks were made:

1. Daily:

(a) The telescope high voltages were checked with an electrostatic voltmeter.

(b) The gains of each of the four telescope counter amplifiers were checked.

(c) Pulses from the four counters were observed on an oscilloscope, and the single counting rates of Counter I and Counter III were checked.

(d) The tank pulse height from each bank was observed when a Na^{22} source was suspended in the beam tube.

2. Every two or three days:

(a) A fission calibration was made.

(b) The high voltages and the amplifier gains of the two tanks were checked.

3. Periodically (about once a month):

(a) Pulse-height distribution measurements from the film were made for Counter II and Counter IV.

(b) Pulse-height and time-distribution measurements were made from the fission-calibration film.

IV. SOURCES OF ERROR

In interpreting the data, there are several necessary assumptions and corrections that should be mentioned. Since we are not able to identify a particular stopping as a μ^- meson nor a particular tank pulse as a neutron, these identifications must be made statistically.

A. Mesons

1. Contamination of Beam

a. Non-μ-mesic contamination

We shall first consider the effect on our data of non-μ-mesic contamination. Uncharged particles do not trip Counter I. The 8 in. of lead between Counters I and II is quite adequate to eliminate electrons and positrons. (Any conceivable shower event that could partially penetrate and also produce the

desired results in Counters II and III would certainly produce an unacceptably large prompt tank pulse). The π-meson flux at sea level is negligible because of the short lifetime of this particle. Therefore, the only contaminants that may be of any consequence are protons. In the energy range of stopping, the P/μ ratio is approximately 0.03.[36] In addition, the absorbing material above Counter III provides almost two mean free paths of attenuation.[36] We have considered the effect on our data from protons to be small but unknown, and no numerical correction has been made.

b. μ^+ mesons

The fraction of stopping mesons that are negative must be calculated from the known μ^+/μ^- ($\equiv r_\pm$) ratio. This was taken to be $r_\pm = 1.21 \pm 0.03$.[37] However, as this appears in the calculation, we have

$$\mu^-/(\mu^+ + \mu^-) = 1/(r_\pm + 1) = 1/(2.21 \pm 0.03)$$

which gives an error negligible compared with the statistical counting error.

2. Fraction of Mesons Captured

Some of the μ^- mesons decay before they can be captured. The fraction that decays can be determined by comparing the μ^- lifetimes (τ_-) when stopped in lead or silver with the known decay lifetime (τ_d) according to the equation

$$1/\tau_- = 1/\tau_c + 1/\tau_d ,$$

where $\tau_c \equiv$ capture lifetime and the fraction that decays before capture equals τ_-/τ_d. The values used in the calculation were $\langle\tau_-\rangle_{Pb} = 0.0745 \pm 0.0083$,[38] $\langle\tau_-\rangle_{Ag} = 0.0844 \pm 0.0035$,[38] and $\tau_d = 2.22 \pm 0.02$,[39] giving $(\tau_-/\tau_d)_{Ag} = 0.038 \pm 0.003$, and $(\tau_-/\tau_d)_{Pb} = 0.034 \pm 0.001$.

B. Neutrons

1. Neutron-Counting Efficiency

The neutron-counting efficiency is the product of two functions:

(a) the probability (Eff') that a neutron produced in the center of the beam tube will give a tank pulse,

(b) the probability that the neutron will not be absorbed by the target--that is, the transmission (T)--

or

$$Eff = Eff' \times T.$$

The probability (Eff') is determined by the ratio

$$\frac{\text{Average number of neutrons observed per } Cf^{252} \text{ fission}}{\text{known average neutron multiplicity from } Cf^{252} \text{ fission}}$$

$$= \frac{\bar{n}\ Cf^{252}}{\bar{\nu}\ Cf^{252}}$$

The value of $\bar{\nu}\ Cf^{252}$ used in the calculation is 3.869 ± 0.078.[40]

T was determined by measuring the activity induced in a solution of M_nSO_4[41] by a mock-fission[42] neutron source with and without a target present. In order to simulate the geometry of the scintillator tank, a commercially available galvanized iron can 30 in. in diameter was filled to a height of 30 in. with the M_nSO_4 solution. In the center of the can, rising vertically, was an 8-in.-diameter iron pipe (the pipe, therefore, was rotated 90° with respect to the tank dimensions and geometry and those of the can), which was closed at the bottom and weighted down with lead bricks. A hole 1.125 in. in diameter and 2.5 in. deep was drilled in the center of each of the targets to accommodate the 1-in.-diameter by 1-in.-high source. For Pb, the ratio of the absorber in to absorber out induced activity was close to unity (0.98 ± 0.02). For Ag, it was smaller, and therefore a third measurement was made, with the source right next to but not inside the target. The measured activity ratios were

$$\text{center of target/no target} = 0.87 \pm 0.02,$$

$$\text{side of target/no target} = 0.94 \pm 0.02.$$

An average transmission for silver was estimated to be 0.91 ± 0.03.

2. Positron Contamination

It was also necessary to verify that the tank pulses observed were actually caused by neutrons. In the study of these pulses they were divided into two groups; one group included the delayed tank pulses accompanied by either a prompt tank pulse or at least one other delayed pulse (Fig 6A). The pulses observed here, after being corrected for background, could be explained only as neutrons. Indeed, we see this to be true when we compare their time distribution with that of delayed tank pulses from Cf^{252} fissions. However, if there is no prompt tank pulse, we may still be seeing neutrons (since the radiation accompanying capture may be absorbed in the target), or we may be seeing

radiation from positrons from $\mu^+ \rightarrow e^+ + \nu + \bar{\nu}$ (Fig. 6B). As can be seen by comparison with Fig. 6A, both these effects were observed, and a separation has been made on the basis of time distribution. In Fig. 7 we have replotted the time distribution of delayed tank pulses for cases in which they appeared alone on the sweep. The 8.65-μsec neutron lifetime can be "peeled off," leaving a time distribution quite consistent with that for μ^+ decay.

In practice, the correction was made by counting the number of tank pulses for times < 8.1 μsec after the stopping and those for times > 8.1 μsec. The ratio of these was compared with the ratio obtained from the Cf^{252} fissions. The excess pulses for t < 8.1 μsec were considered to be due to μ^+ decay.

3. Accidentals

The accidental tank pulses were monitored in two ways. The oscilloscope viewing the tank photomultiplier tubes was triggered by a relaxation oscillator with approximately a 3-min time constant (as compared with the coincidence rate of about one every 2 min). The tank pulse rate observed on these artificially triggered sweeps was recorded, and the tank pulse rate observed when a meson passed through the target was also recorded. In both these cases the rates were found, within statistical error, to be the same, and the pulses were observed to occur randomly in time. Therefore, the pulses associated with a meson passing through the target also represented accidentals. The values used in the calculations were those from the pass-through events. Because the pass-throughs are statistically proportional to the number of stoppings, the average accidental rate for a series of rolls of film could be obtained simply by taking the ratio of the total accidental tank pulses to the total pass-throughs.

V. EXPERIMENTAL RESULTS AND ANALYSIS

A. Results

Before presenting the experimental data, we should explain the choice of targets. Originally, it was intended to perform the experiment on a spectrum of atomic numbers. Four elements were chosen on the basis of a compromise between availability and high density (which, for given dimensions and atomic number, means high stopping power). These elements were Al, Cu, Ag, and Pb. Shortly after the commencement of the experiment, it was decided to concentrate on better statistics for the multiplicity distributions, and hence

only the two targets promising the highest neutron yields were used, namely Pb and Ag.

The experimentally determined neutron-multiplicity values together with some other pertinent parameters are given in Table I. The reduced data are given in Table II.

B. Analysis

1. Comparison with Theory

In assigning numerical values to the parameters in Eq. (5) and (6), we calculated $p_o(q_o)$, the maximum neutron (proton) momentum of the Fermi sphere, from the relationship

$$p_o(q_o) = \frac{\hbar}{r_0}\left(\frac{Z(N)}{A}\ \frac{9\pi}{4}\right)^{1/3}, \qquad (8)$$

where the nuclear radius, equals $r_0 A^{1/3}$ and r_0 is taken to be 1.2×10^{-13} cm.[43] The values used for BE_μ were 10.5 Mev for Pb and 5 Mev for Ag.[44] The nuclear mass differences, ΔM, are given in Table III.

Integrals of the form $\int_{B_\nu}^{\infty} N_\nu I(Q)\,dQ$ were evaluated; the probability of emission of ν neutrons, I_ν, was

$$I_\nu = \int_{B_\nu}^{\infty} N_\nu I(Q)\,dQ - \int_{B_{\nu+1}}^{\infty} N_{\nu+1}\, I(Q)\,dQ.$$

The calculated results were all obtained by numerical integration of the above expression.

The derived values of I_ν were then averaged over the respective natural abundances of the isotopes of Pb[45] and Ag and converted to observation probabilities, f_n. The values of f_n --the distributions we would expect to observe when we have observation efficiency ϵ -- and the actual distributions, I_ν, are expressed by the equation

Table I

Experimentally determined neutron-multiplicity values and other pertinent parameters

	Target		
	Pb	Ag	None
Incident beam (total coincidences)	22,842	19,069	21,517
Total stops	909	839	108
Absorbing material in g/cm^2 Pb equiv.*	123.8	135.5	12.3
Relative stops per unit beam	1	1.106	0.114
Relative stopping power (computed)	1	1.095	0.091
Minimum energy to trigger coincidence (Mev)	380	380	380
Corresponding momentum (Mev/c)	475	475	475
Maximum energy to stop (Mev)	525	535	395
Corresponding momentum (Mev/c)	625	635	490
Background pulses per stop	0.064	0.053	0.051
Net efficiency (Eff = Eff'xT)	57.7	50.8	53.6
Tank pulses from μ^+ decays	114 ± 15	134 ± 15	33 ± 6
N_0 (No. of stops with no tank pulse)	512	479	55
N_1 (No. of stops with one tank pulse)	305	293	46
N_2 (No. of stops with two tank pulses)	69	51	4
N_3 (No. of stops with three tank pulses)	14	12	3
N_4 (No. of stops with four tank pulses)	5	2	0
N_5 (No. of stops with five tank pulses)	2	0	0
N_6 (No. of stops with six tank pulses)	1	0	0
N_7 (No. of stops with seven tank pulses)	1	2	0

*The absorbing material included, in addition to the targets, a 2-in. plastic scintillator (Counter III), and 0.0625-in. copper and 0.125-in. aluminum supporting pieces. The total absorber had an effective stopping power of 12.3 g/cm^2 Pb equivalent.

Table II

Relative neutron multiplicities from μ^- capture

A. In lead (adjusted to 57.7% detection efficiency)

Neutron multiplicity probabilities	Observed	Theoretical			
		Alpha particle	Fermi gas		
			$M^* = M$ $\theta_F = 0$	$M^* = M/2$ $\theta_F = 0$	$M^* = M/2$ $\theta_F = 10$ Mev
f_0	0.32±0.10	0.325	0.53	0.34	0.43
f_1	0.49±0.06	0.363	0.46	0.48	0.42
f_2	0.15±0.03	0.181	0.01	0.18	0.14
f_3	0.019±0.014	0.078	0	0.006	0.012
f_4	0.011±0.006	0.032		0	<0.001
f_5	0.006±0.005	0.013			
f_6	0.003±0.003	0.004			
f_7	0.003±0.003	0.001			
Av. neutrons observed per capture					
$\bar{n}$	0.94±0.09	1.18	0.48	0.86	0.73
Av. neutrons emitted per capture					
$\bar{\nu}$	1.64±0.16	2.06	0.84	1.48	1.26

B. In silver (adjusted to 50.8% detection efficiency)

f_0	0.42±0.10	0.433	0.37
f_1	0.44±0.07	0.362	0.46
f_2	0.11±0.03	0.134	0.16
f_3	0.025±0.012	0.050	0.017
f_4	0.003±0.002	0.015	0
f_5	0.006±0.004	0.004	
f_6	0	0.001	
f_7	0.006±0.004		
$\bar{n}$	0.81±0.09	0.86	0.83
$\bar{\nu}$	1.60±0.18	1.70	1.64

Table III

A. Neutron binding energies

Isotope of Thallium 48	Binding energy (Mev)	Isotope of Palladium 49	Binding energy (Mev)
Tl^{208}		Pd^{109}	
	3.86		6.2
Tl^{207}		Pd^{108}	
	6.97		9.1
Tl^{206}		Pd^{107}	
	6.23		6.2
Tl^{205}		Pd^{106}	
	7.48		9.6
Tl^{204}		Pd^{105}	
	6.54		7.1
Tl^{203}		Pd^{104}	
			9.8
		Pd^{103}	

B. Nuclear mass differences 50

Isotopes	ΔM (Mev)
Tl^{208} - Pb^{208}	5.50
Tl^{207} - Pb^{207}	1.95
Tl^{206} - Pb^{206}	2.02
Pd^{109} - Ag^{109}	1.56
Pd^{107} - Ag^{107}	0.55

$$f_n = \sum_{\nu=n}^{\infty} I_\nu \epsilon^n (1-\epsilon)^{\nu-n} \binom{\nu}{n}.$$

The calculated values of f_n for Pb, tabulated together with the experimental results in Table II, are shown graphically in Fig. 8. Looking at the results for Pb, we see that a degenerate-Fermi-gas model with $M^* = M$ is completely inadequate to explain the multiplicities.

With $M^* = M/2$, the calculated values agree fairly well in the lower multiplicities with those observed. Excitation of the gas to 10 Mev, although introducing a finite probability for high excitation, actually tends to decrease the average multiplicity because lower-energy final states that were previously excluded are now made available.

The α-particle model, on the other hand, differs by several standard deviations from experiment for the multiplicities f_1 and f_3. The observation of the higher multiplicities cannot be explained by the Fermi gas model, whereas the α-particle model predicts multiplicities even higher than are observed.

Although one of these two descriptions may provide a distinctly better approximation to the physical situation, the experimental information is not sufficiently complete to allow us to make a clear separation. We are limited by a small but unknown effect of nucleon contamination and a lack of knowledge about the neutron energy spectrum.

For example, in Pb, the number of stoppings accompanied by four or more observed neutrons amounts to only 1% of the total, in Ag to only 0.5%. It would not be unreasonable to assume that this comparatively small fraction of events is caused by proton contamination.[46] From the other point of view, if there are high neutron excitations they will not necessarily always be manifested as large neutron multiplicities. The greater the energy of the produced neutron, the longer its mean free path in nuclear matter and, hence, the more likely it is to leave the nucleus as a high-energy neutron. This effect would tend to increase single-neutron emission at the expense of higher multiplicities.

A comparison of the calculated multiplicity distributions for Ag with those observed gives qualitatively similar results (Fig. 9). However, it is more difficult to make a sharp distinction between the relative fits of the Fermi gas model ($M^* = M/2$, $\theta_F = 0$) and the α particle model, since both models predict the same average multiplicity; and, because of the decreased counting

efficiency for this target, differences in prediced multiplicity distributions are less pronounced.

It should be noted that in the Fermi gas model used, a higher average neutron multiplicity is predicted for Ag than for Pb. The reason for this is that the model predicts higher proton momenta ($p_o^3 \propto Z/A$, Eq. 8), and therefore higher nuclear excitations for Ag than for Pb. This effect is not observed, but is statistically compatible with the observations.

2. Comparison with Other Experiments

There are no previous experimental results on the average neutron multiplicities for Ag. The average neutron multiplicities previously reported for Pb are:

University of Chicago,[17] $\bar{\nu} = 1.96 \pm 0.72$;
Washington University,[47] $\bar{\nu} = 1.7 \pm 0.3$;
Cornell University,[20] $\bar{\nu} = 2.14 \pm 0.13$,

The first two results are compatible with ours. However, Widgoff at Cornell obtained a value 30% higher. One possible explanation for this disagreement may be a counting efficiency discrepancy due to the difference between the neutron energy spectrum of μ^--capture neutrons and that from a Ra-Be source used for efficiency calibration of Widgoff's BF_3 counters. In her paper she suggests that this might introduce a systematic error as high as 20%.

Having available a Ra-Be as well as a mock-fission source, we decided to test the sensitivity of a BF_3 counter's efficiency to neutron energy spectrum. To do this we built a paraffin structure with a rectangular tunnel through the center (Fig. 10). A hole large enough to accommodate a BF_3 counter was drilled lengthwise through one of the paraffin blocks forming the structure. By rearranging its position with respect to the other blocks we varied the distance of the BF_3 counter from the tunnel, although keeping it always imbedded in the paraffin. The neutron counting rate as a function of distance from the tunnel was recorded for both sources. The neutron yields were normalized to one another by determining their relative activities with the previously mentioned $MnSO_4$ tank. These results are also plotted in Fig. 10. We see that a discrepancy of as high as 25 to 30% is indicated for a counter 1.5 to 2.5 in. inside the paraffin. That is, a counter whose efficiency was calibrated at this distance with a Ra-Be source would actually be 25 to 30%

more efficient in detecting fission-spectrum neutrons. A "boil off" neutron spectrum should be more closely approximated by a fission spectrum.

VI. CONCLUSIONS

Upon examination of the neutron multiplicity distribution from μ^--meson capture in heavy nuclei, we obtain results which, though not inconsistent with an α-particle model, seem to better fit a Fermi gas model with the effective nucleon mass, M^*, set equal to $M/2$. A clear-cut decision as to which type of description better fits the physical reality requires either neutron energy-spectrum data or better evidence for the presence or absence of the higher neutron multiplicities. For the latter a μ^--meson beam containing less than 0.1% π-meson or nucleon contamination is needed.

At present, investigations are under way to obtain and demonstrate the purity of such a beam from the newly remodeled 184-in. cyclotron.

ACKNOWLEDGMENTS

The authors would like to thank Professor Edward Teller for suggesting the problem and to acknowledge the help extended by a number of other people in the course of this research: Dr. George Millburn; Dr. Warren Heckrotte for his advice on the theoretical portion; Dr. Francis Cole, who was kind enough to lend us a personal copy of his thesis; Dr. Stanley Thompson, for supplying the Cf^{252} source; and the people who read the film, Lucy Lienesch and Knoxie DeLise.

REFERENCES

1. M. H. Johnson and E. Teller, Phys. Rev. 98, 783 (1955).
2. K. A. Brueckner, Phys. Rev. 97, 1353 (1955).
3. H. A. Bethe, Phys. Rev. 103, 1353 (1956).
4. E. Fermi and E. Teller, Phys. Rev. 72, 399 (1947).
5. J. A. Wheeler, Revs. Modern Phys. 21, 133 (1949).
6. L. N. Cooper, and E. M. Henley, Phys. Rev. 92, 801 (1953).
7. V. Fitch and L. J. Rainwater, Phys. Rev. 92, 789 (1953).
8. M. Conversi, E. Pancini, and O. Piccioni, Phys. Rev. 71, 209 (1947).
9. H. K. Ticho, Phys. Rev. 74, 1337 (1948).
   Keuffel, Harrison, Godfrey, and Reynolds, Phys. Rev. 87, 942 (1952).
   A. Alberigi-Quaranta and E. Pancini, Nuovo cimento 11, 607 (1954).
   A number of other references are given by Sard and Crouch.
10. W. F. Fry, Phys, Rev. 90, 999 (1953).
11. J. Steinberger and H. B. Wolfe, Phys. Rev. 100, 1490 (1955).
12. O. Piccioni, Phys. Rev. 74, 1754 (1948).
13. W. Y. Chang, Revs. Modern Phys. 21, 166 (1949).
14. H. Morinaga and W. F. Fry, Nuovo cimento 10, 308 (1953).
15. Sard, Ittner, Conforto, and Crouch, Phys. Rev. 74, 97 (1948).
16. G. Groetzinger and G. W. McClure, Phys. Rev. 74, 341 (1948).
17. Groetzinger, Berger, and McClure, Phys. Rev. 81, 969 (1951).
18. A. M. Conforto, and R. D. Sard, Phys. Rev. 85, 120 (1952).
19. A. M. Conforto and R. D. Sard, Phys. Rev. 86, 465 (1952).
20. M. Widgoff, Phys. Rev. 90, 892 (1953).
21. J. Tiomno and J. A. Wheeler, Revs. Modern Phys. 21, 153 (1949).
22. M. N. Rosenbluth, Phys. Rev. 75, 532 (1949).
23. J. M. B. Lang, Proc. Phys. Soc. (London) A65, 995 (1952)
24. Francis T. Cole, The Capture of Negative Mu Mesons by Atomic Nuclei, Thesis, Cornell University, 1953.
25. Hicks, Ise, and Pyle, Phys. Rev. 101, 1016 (1956).
26. Cladis, Hess, and Moyer, Phys. Rev. 87, 425 (1952)
27. J. M. Wilcox and B. J. Moyer, Phys. Rev. 99, 875 (1955).
28. This was an arbitrary choice for illustrative purposes. cf. A. Rosenfeld, Nuclear Forces II § 12.22 and J. Heideman, Phys. Rev. 80, 171 (1950).

REFERENCES (Cont.)

29. J. M. Blatt and V. Weisskopf, Theoretical Nuclear Physics (Wiley, New York, N. Y. 1952) Ch. VIII.
30. E. R. Graves and L. Rosen, Phys. Rev. 89, 343 (1953).
31. Cole argues that the average energy corresponding to the emission of one neutron would be $\simeq 1/2 (B_1 + B_2)$ if two neutrons were always emitted at B_2. However, because "the neutrons are actually emitted with some kinetic energy (average 1 to 2 Mev), one should add about 2 Mev to $1/2 (B_1 + B_2)$". Hence we have $1/2 (B_1 + B_2) + 2$.
32. The pulse-height range was chosen by making a height-distribution measurement of the Counter II pulses for events where the particle also passed through Counter IV (minimum ionization in Counter II). Inclusion of more than 90% of the pulses required a range of acceptance of H of 30% H, where H was the average pulse height, representing a minimum ionization-energy loss of 55 Mev.
33. Reines, Cowan, Harrison, and Carter, Rev. Sci. Instr. 25, 1061 (1954).
34. Hays, Ott, and Ken, Nucleonics 14, No. 1, 42 (1956).
35. G. Bartholomew and B. Kinsey, Phys. Rev. 90, 355 (1953); Can. J. Phys. 31, 1051 (1953); and H. Motz, Phys. Rev. 90, 355 (1953).
36. M. G. Mylroi, and J. G. Wilson, Proc. Phys. Soc. A64, 404 (1951).
37. Robert Brode, University of California, private communication.
38. A. J. Meyer, Contract N6CNR-27-II Tech. Rep. No. 16 (NP54/8) Quoted in Nucl. Sci. Abstr. 9-721.
39. W. E. Bell, and E. P. Hinks, Phys. Rev. 84, 1243 (1951).
40. Diven, Martin, Taschek, and Terrell, Phys. Rev. 101, 1012 (1956).
41. A description of the $MnSO_4$ technique can be found in Crandall, Millburn, and Schecter, J. Appl. Phys. 28, 273 (1957).
42. This is a source manufactured commercially by the Mound Laboratories of the Monsanto Chemical Co. It consists of Po, Be, B, Li, and F mixed in proper proportions so that the resultant neutron spectrum resembles that from fission with respect to both average energy and shape.
43. L. Wilets, Phys. Rev. 101, 1805 (1956).
44. The exact values for BE_μ are not critical to the calculation. Our numbers were obtained by extrapolation of the experimental and theoretical values found in Ref. 7.

45. Pb^{204}, which is only 1.5% abundant, was neglected in the calculation, and the relative abundances of the other isotopes were adjusted proportionally to give 100%.

46. For example, a 200-Mev proton interacting in Pb may be expected to give an average neutron multiplicity of ≃ 6. cf. W. Crandall, and G. Millburn, UCRL-2706 (1954).

47. R. D. Sard and M. F. Crouch, Progress in Cosmic Ray Physics, Vol. II (Interscience, New York, 1952) p. 3

48. J. A. Harvey, Phys. Rev. 81, 353 (1951), (Table II).

49. Complete experimental data were not available here but a consistent-looking set of values was compiled from the experimental and theoretical data in the following sources:

American Inst. of Phys. Handbook (McGraw-Hill, New York, 1957); B. E. Cushman, Isotopic Masses: A Guide to the Literature, UCRL-2468, Jan. 1954; and J. Riddell, Chalk River Proj. Rept. CRP-654 (1956).

50. Hollander, Perlman, and Seaborg, Table of Isotopes, UCRL-1928 (Rev.), Dec. 1952.

LEGENDS

Fig. 1. Nuclear-excitation distributions from μ-meson capture, as predicted by the various theoretical models.

Fig. 2. The probability for the emission of at least ν neutrons as a function of the nuclear excitation in excess of the binding energy of ν neutrons, $\delta_\nu \Theta = Q - B\nu$.

Fig. 3. Experimental counter geometry. A and C represent alternate target arrangements used during part of the Pb run to determine whether any systematic errors could be caused by Coulomb scattering. No such effect was observed.

Further evidence for the absence of such an effect is the good agreement between the observed and calculated relative meson stopping rates in Pb and Ag (Table I).

Fig. 4. Drawings of typical oscilloscope traces.

Fig. 5. Block diagram of electronics.

Fig. 6. Time distribution of delayed tank pulses. A is accompanied by at least one other pulse on the sweep, and B is alone on the sweep. The time distribution of pulses from Cf^{252} fission is shown for comparison.

Fig. 7. Separation of μ^+ decay pulses from neutron pulses.

Fig. 8. Comparison of the observed neutron multiplicities from lead with theoretical histograms.

Fig. 9. Comparison of the observed neutron multiplicities from silver with theoretical histograms. Only the Fermi gas histogram providing the best fit is reproduced. Its relationship to the other Fermi gas histogram can be inferred from the corresponding graphs for Pb (Fig. 8).

Fig. 10. Relative efficiencies for detection of neutrons from a Ra-Be and a mock fission source. The experimental arrangement was similar to that used by previous experimenters for neutron-detection-efficiency calibrations.

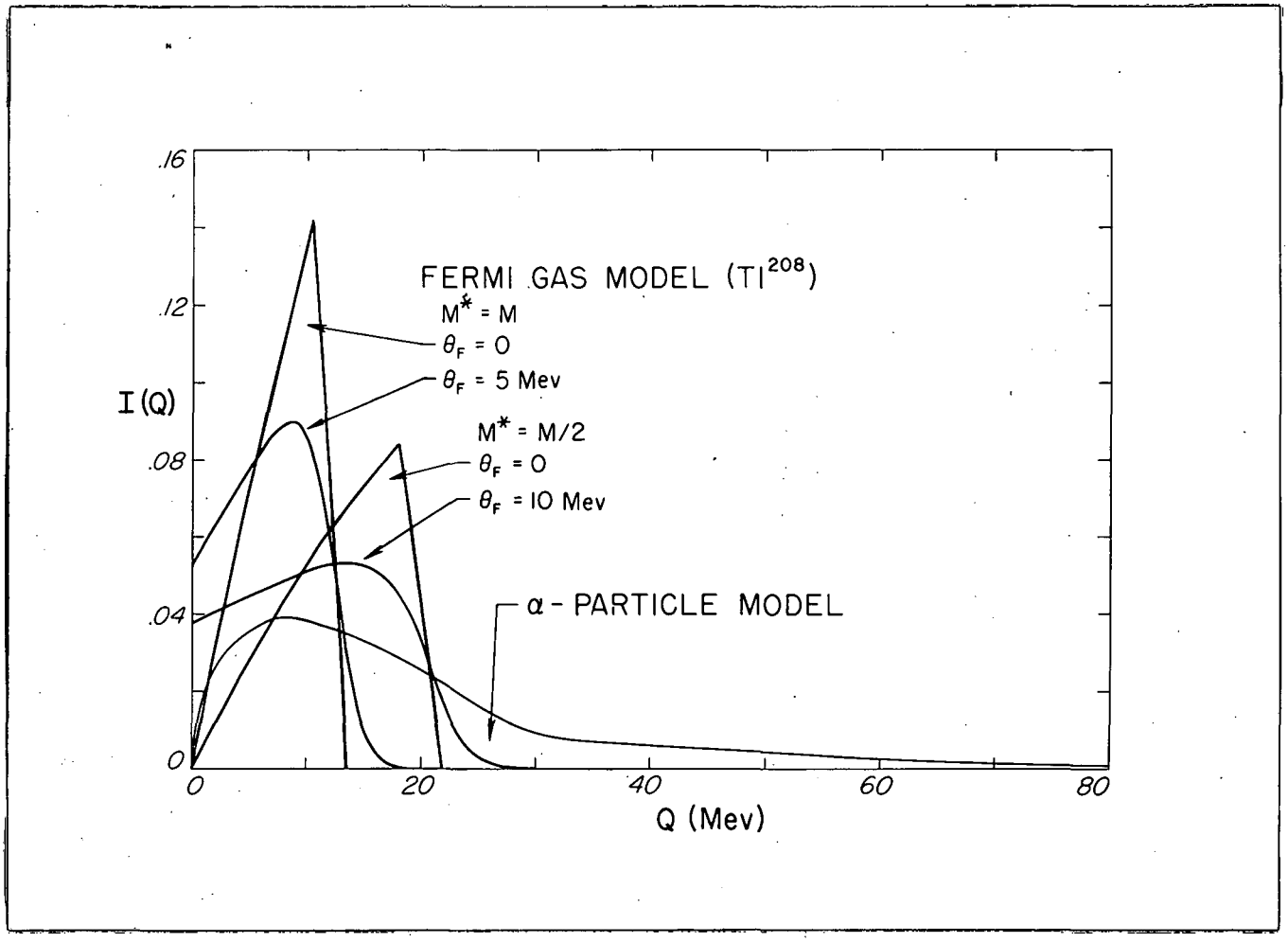
FERMI GAS MODEL (TI^{208})
$M^* = M$
$\theta_F = 0$
$\theta_F = 5$ Mev
$M^* = M/2$
$\theta_F = 0$
$\theta_F = 10$ Mev
α - PARTICLE MODEL
I(Q)
Q (Mev)
.16
.12
.08
.04
0
0
20
40
60
80

Fig. 1

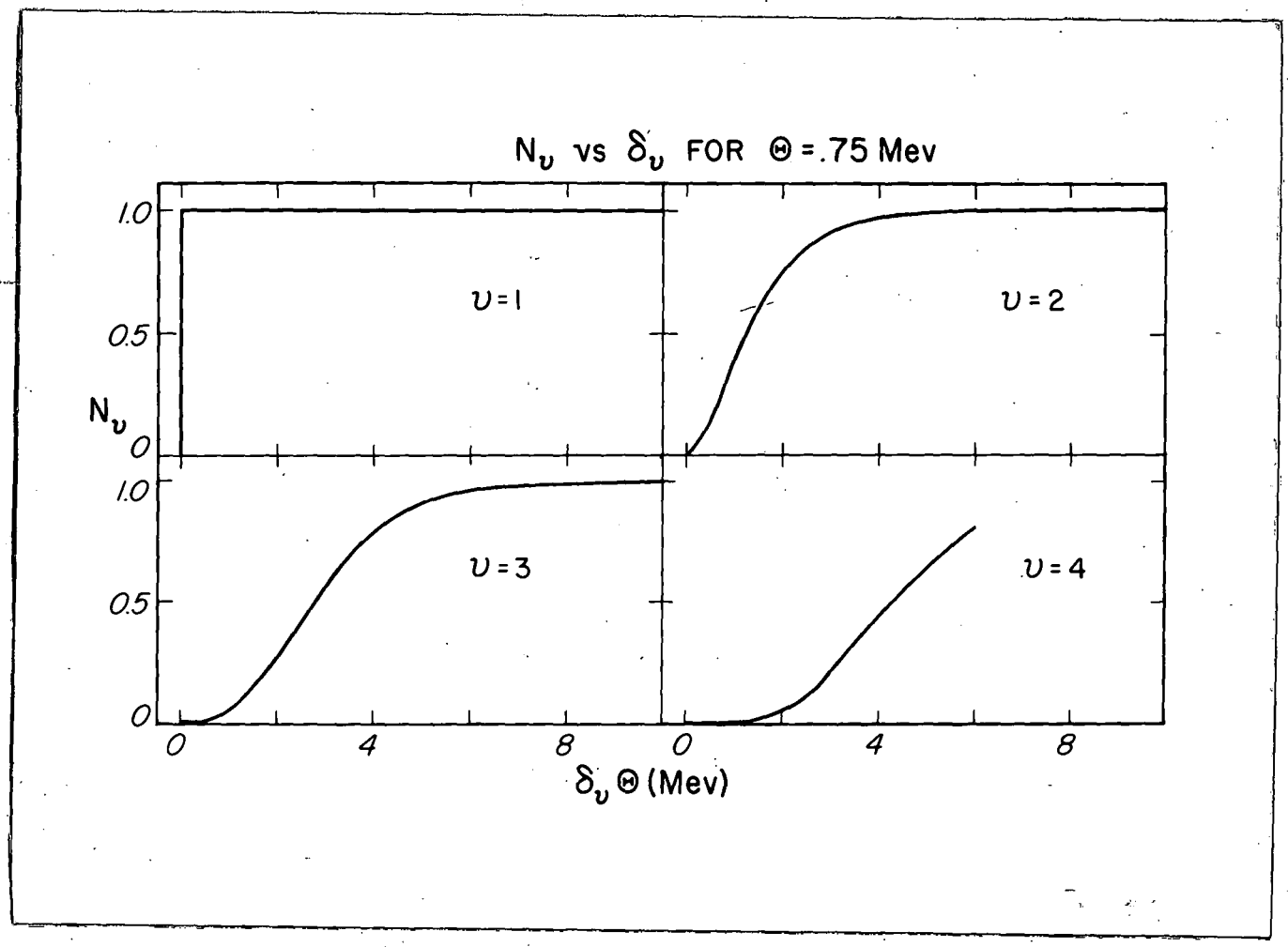
N_υ vs δ_υ FOR Θ = .75 Mev
1.0
0.5
N_υ
0
υ = 1
υ = 2
υ = 3
υ = 4
0
4
8
$\delta_\upsilon \Theta$ (Mev)

Fig. 2

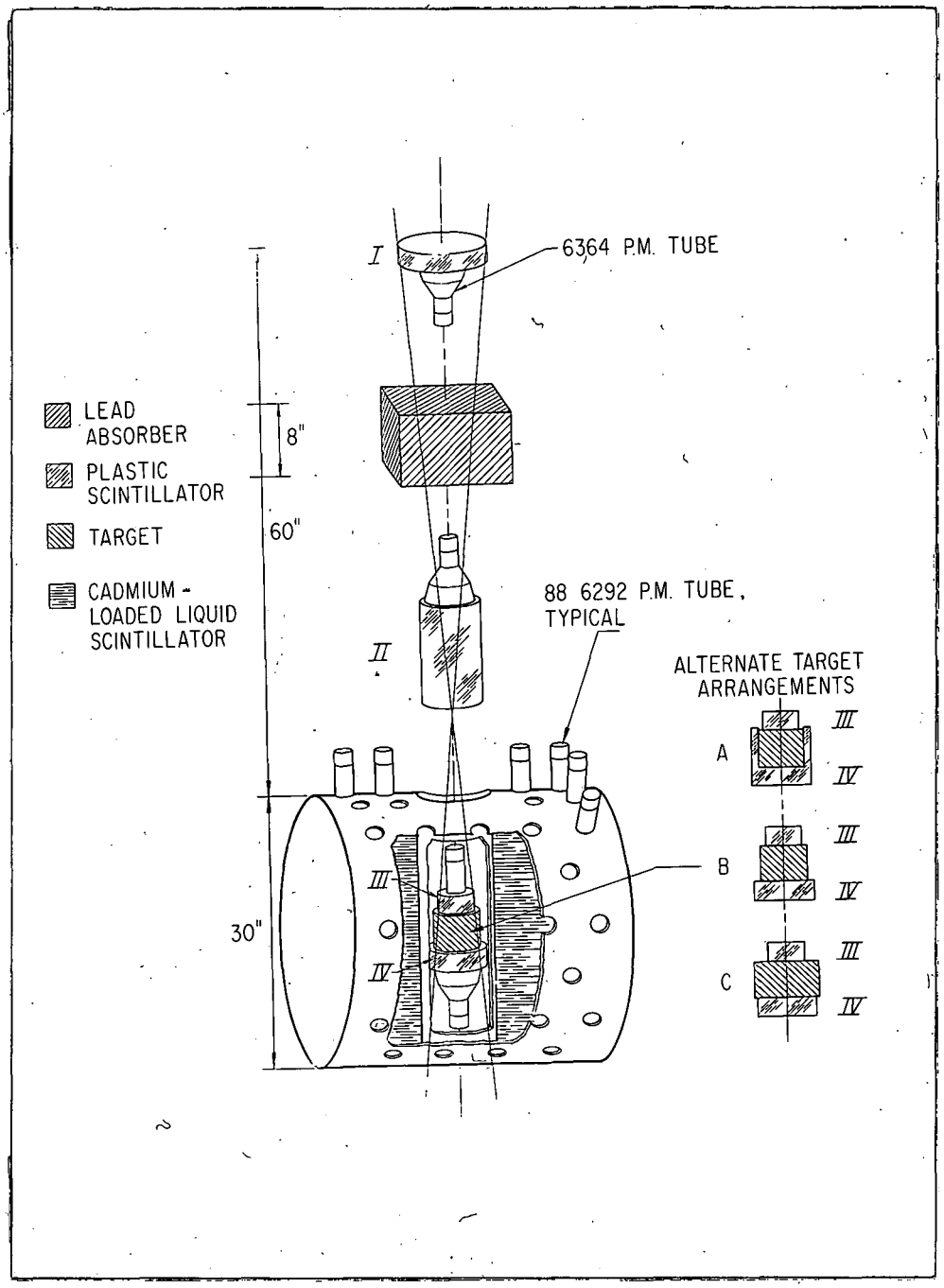
LEAD ABSORBER
PLASTIC SCINTILLATOR
TARGET
CADMIUM - LOADED LIQUID SCINTILLATOR
8"
60"
30"
I
II
III
IV
6364 P.M. TUBE
88 6292 P.M. TUBE, TYPICAL
ALTERNATE TARGET ARRANGEMENTS
A
B
C

Fig. 3

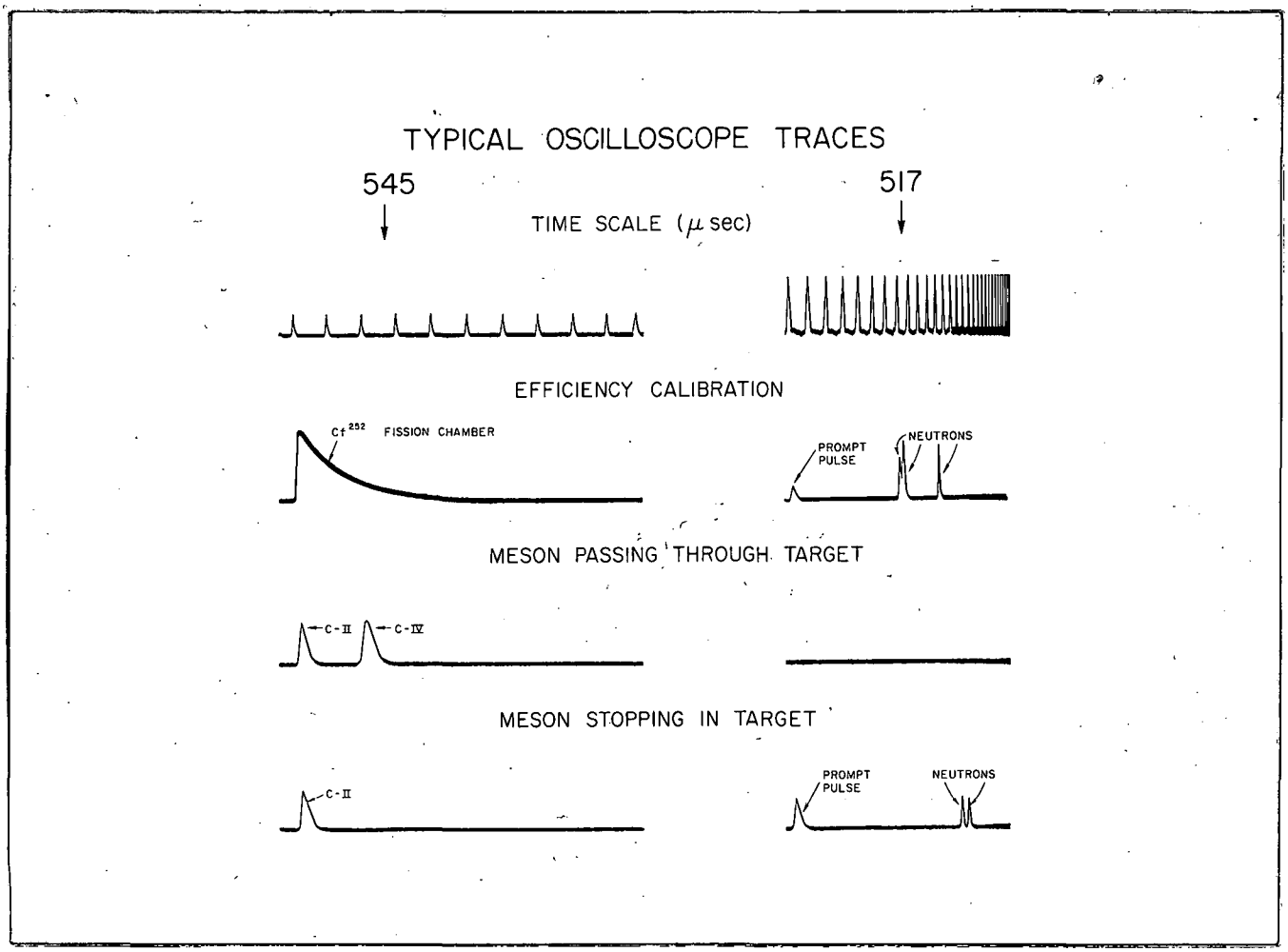
TYPICAL OSCILLOSCOPE TRACES
545
517
TIME SCALE (μ sec)
EFFICIENCY CALIBRATION
Cf 252 FISSION CHAMBER
PROMPT PULSE
NEUTRONS
MESON PASSING THROUGH TARGET
C-II
C-IV
MESON STOPPING IN TARGET
C-II
PROMPT PULSE
NEUTRONS

Fig. 4

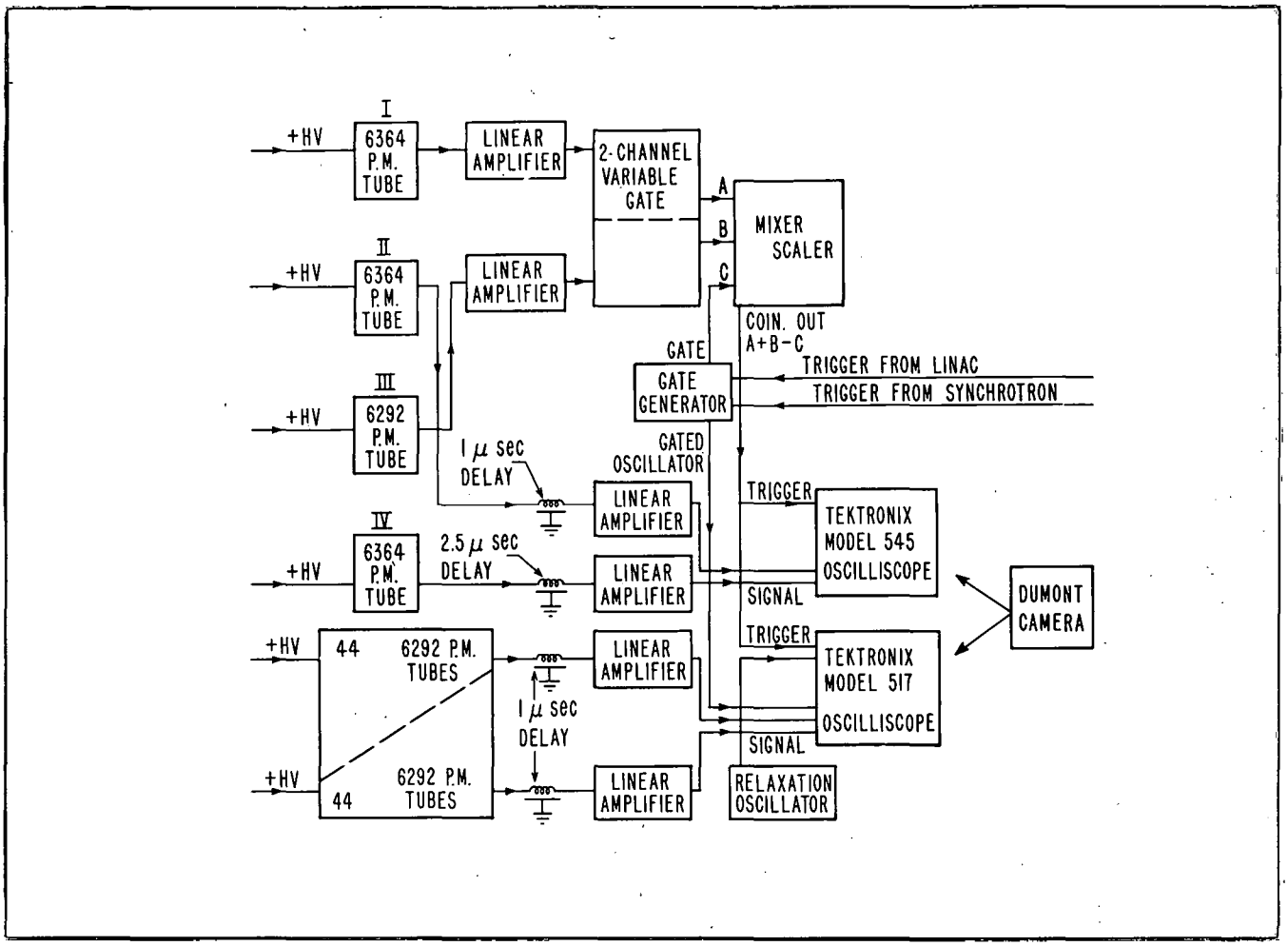
I
+HV
6364 P.M. TUBE
LINEAR AMPLIFIER
2-CHANNEL VARIABLE GATE
A
B
C
MIXER SCALER
II
+HV
6364 P.M. TUBE
LINEAR AMPLIFIER
COIN. OUT A+B-C
GATE
TRIGGER FROM LINAC
GATE GENERATOR
TRIGGER FROM SYNCHROTRON
III
+HV
6292 P.M. TUBE
1 μ sec DELAY
GATED OSCILLATOR
TRIGGER
LINEAR AMPLIFIER
TEKTRONIX MODEL 545 OSCILLISCOPE
IV
+HV
6364 P.M. TUBE
2.5 μ sec DELAY
LINEAR AMPLIFIER
SIGNAL
DUMONT CAMERA
+HV
44
6292 P.M. TUBES
LINEAR AMPLIFIER
TRIGGER
TEKTRONIX MODEL 517 OSCILLISCOPE
1 μ sec DELAY
SIGNAL
+HV
44
6292 P.M. TUBES
LINEAR AMPLIFIER
RELAXATION OSCILLATOR

Fig. 5

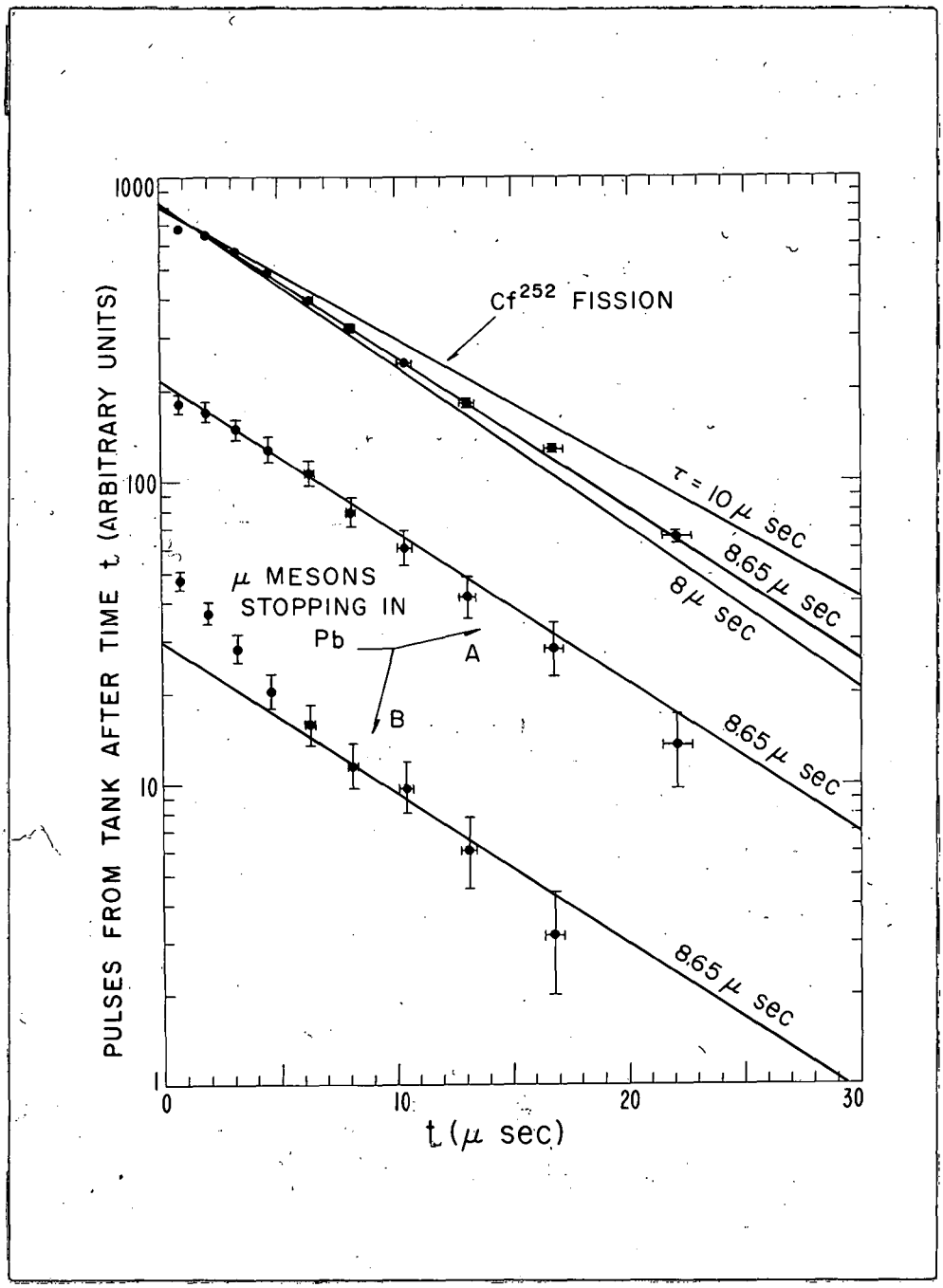
1000
100
10
1
0
10
20
30
PULSES FROM TANK AFTER TIME t (ARBITRARY UNITS)
t (μ sec)
Cf252 FISSION
τ = 10 μ sec
8.65 μ sec
8 μ sec
μ MESONS
STOPPING IN
Pb
A
B
8.65 μ sec
8.65 μ sec

Fig. 6

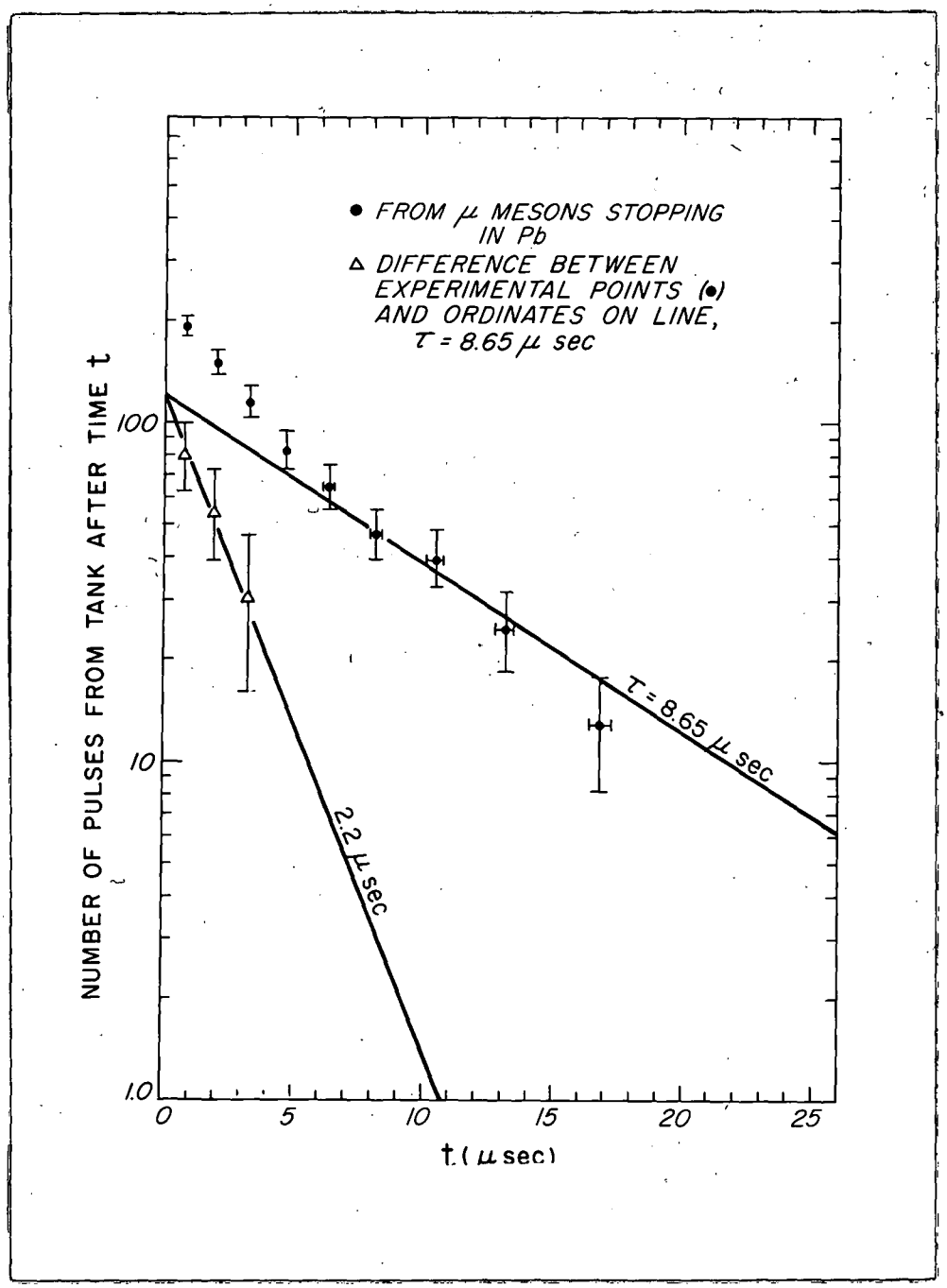
● FROM μ MESONS STOPPING IN Pb
△ DIFFERENCE BETWEEN EXPERIMENTAL POINTS (●) AND ORDINATES ON LINE, τ = 8.65 μ sec
NUMBER OF PULSES FROM TANK AFTER TIME t
100
10
1.0
0
5
10
15
20
25
t (μ sec)
τ = 8.65 μ sec
2.2 μ sec

Fig. 7

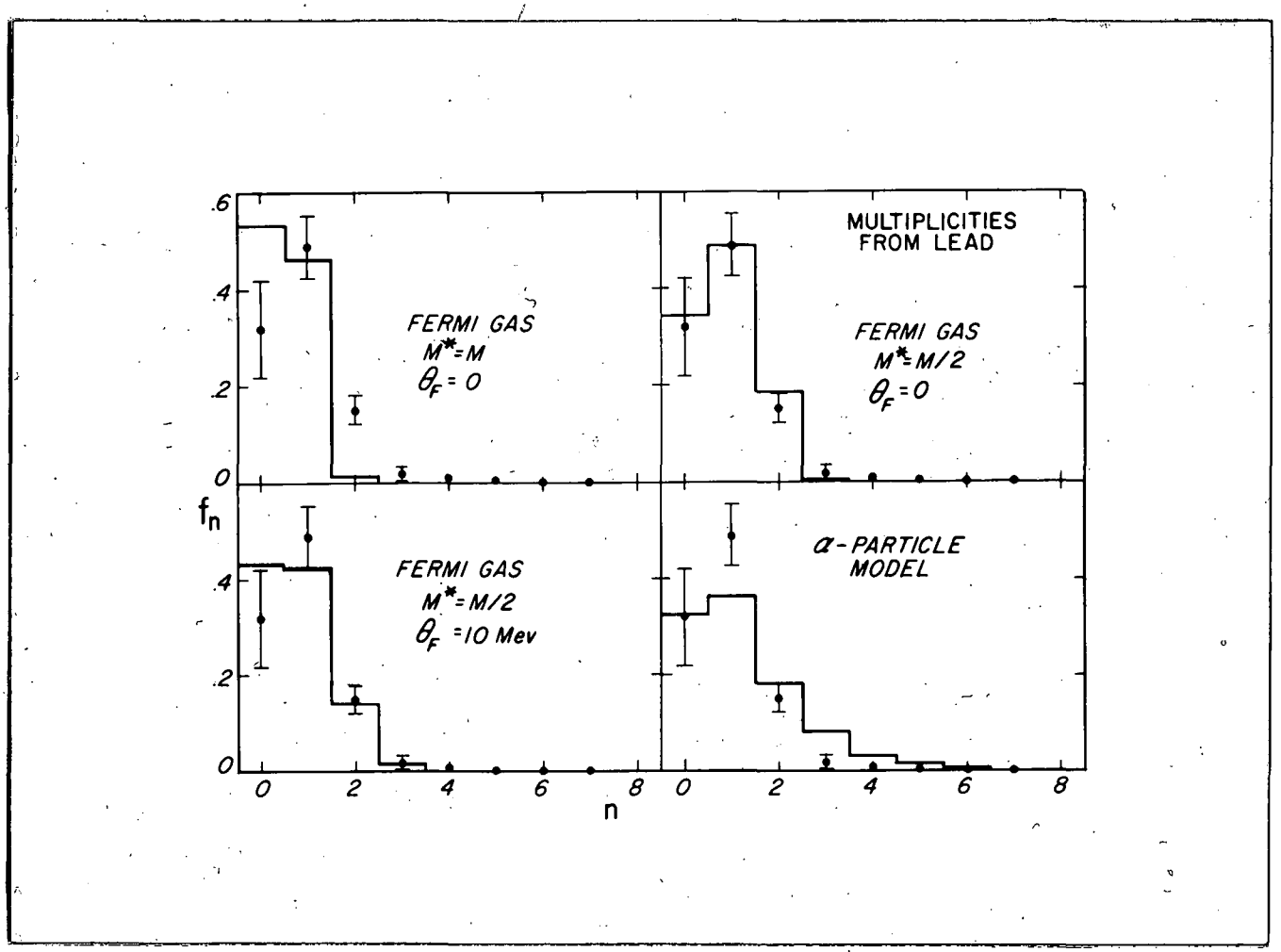
MULTIPLICITIES FROM LEAD
FERMI GAS
M*=M
θF = 0
FERMI GAS
M*=M/2
θF = 0
FERMI GAS
M*=M/2
θF =10 Mev
α-PARTICLE MODEL
fn
n
.6
.4
.2
0
0
2
4
6
8

Fig. 8

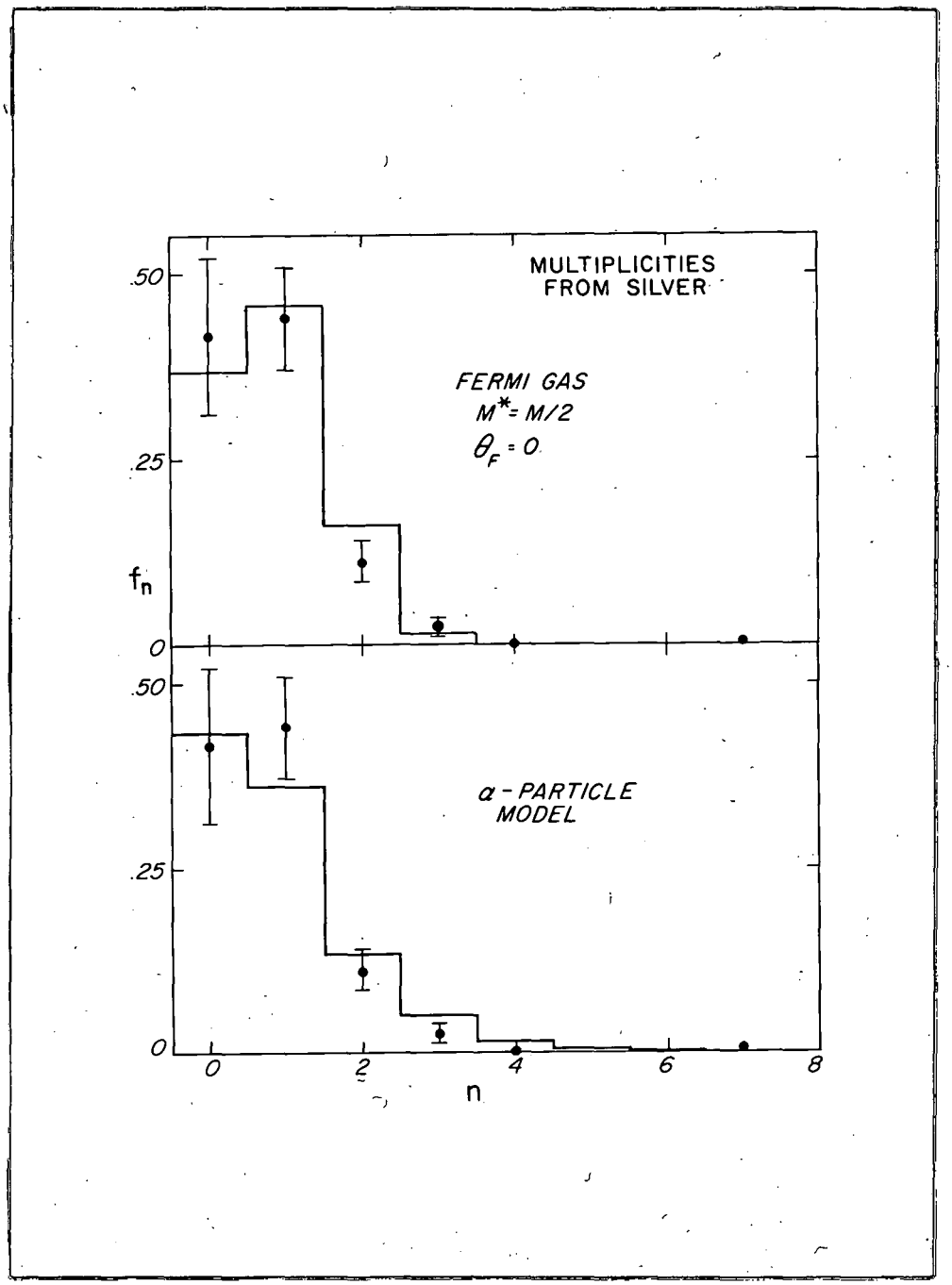
MULTIPLICITIES
FROM SILVER
FERMI GAS
M* = M/2
θF = 0
α - PARTICLE
MODEL
fn
.50
.25
0
.50
.25
0
0
2
4
6
8
n

Fig. 9

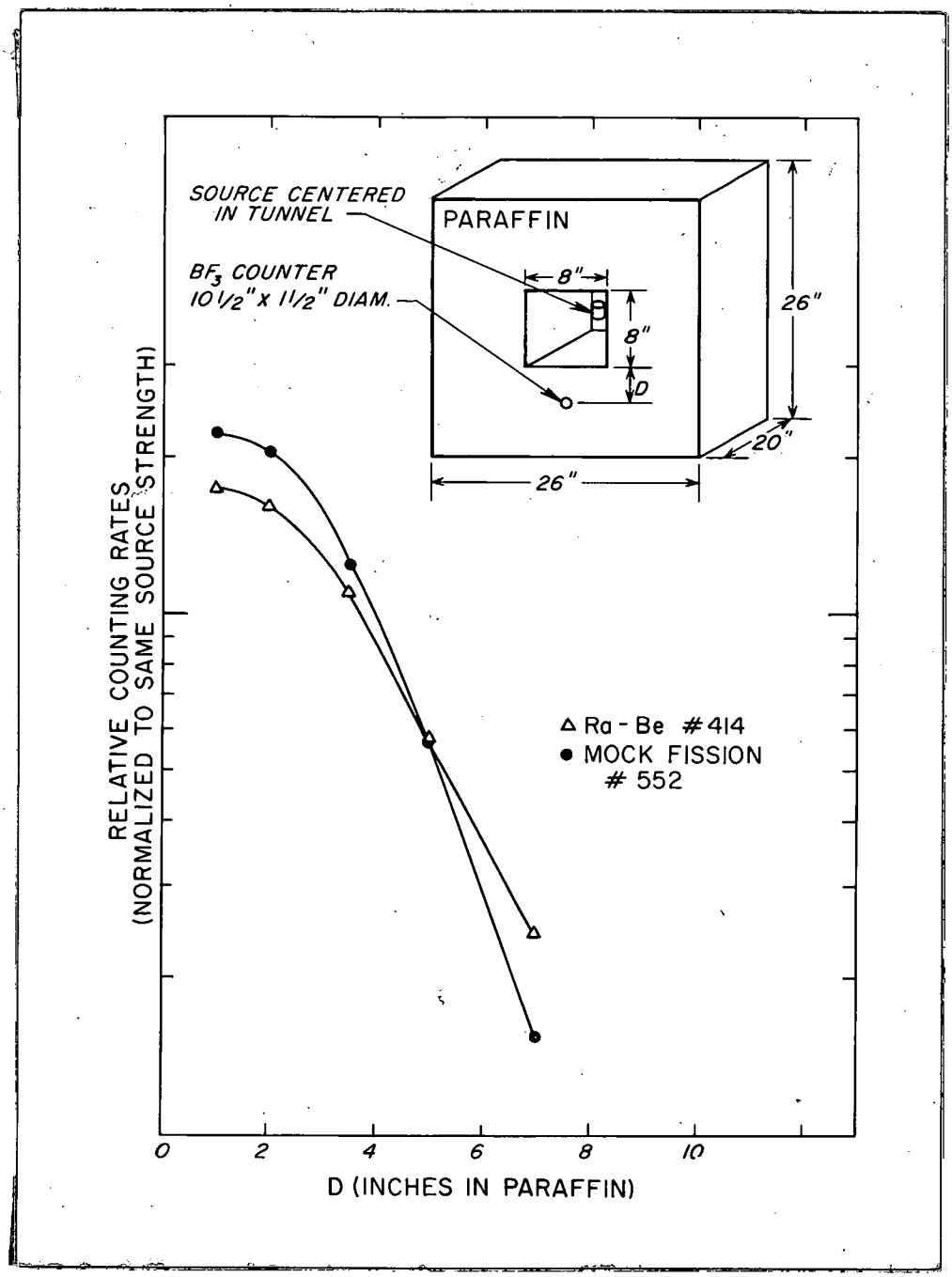
SOURCE CENTERED IN TUNNEL
PARAFFIN
BF_3 COUNTER 10 1/2" x 1 1/2" DIAM.
8"
8"
D
26"
20"
26"
RELATIVE COUNTING RATES (NORMALIZED TO SAME SOURCE STRENGTH)
△ Ra - Be #414
● MOCK FISSION # 552
0
2
4
6
8
10
D (INCHES IN PARAFFIN)

Fig. 10